# Hierarchical Bandwidth Modulation for Ultra-broadband Terahertz Communications

**Zahed Hossain** and **Josep Miquel Jornet**

Department of Electrical Engineering, University at Buffalo, The State University of New York,
Buffalo, New York 14260, USA, E-mail: {zahedhos, jmjornet}@buffalo.edu

***Abstract*—Terahertz (THz)-band (0.1-10 THz) communication has been envisioned as a key technology to enable wireless Terabit-per-second (Tbps) links. At THz frequencies, the path-loss is governed by the spreading loss and the molecular absorption loss. The latter also determines the available transmission bandwidth, which drastically shrinks with distance. New physical layer solutions that capture this behavior are needed to maximally utilize the THz band. In this paper, the concept of hierarchical bandwidth modulation is introduced for single-transmitter multiple-receiver communication in the THz band. In the proposed modulation scheme, multiple flows of information aimed at users at different distances are transmitted at the same time and over the same frequency, by simultaneously adapting both the modulation order and, more importantly, the symbol time. Details for the modulator and the demodulator implementations are provided. The performance of the proposed modulation is analytically derived, both in terms of the achievable data rate as well as symbol error rate. Extensive numerical results based on analytical channel models that capture the peculiarities of the THz band are provided to illustrate the performance of the proposed scheme. The results show that the proposed modulation scheme can maximize the utilization of the distance-dependent bandwidth of the THz channel, turning molecular absorption into an advantage.**

## I. Introduction

Over the last decade, wireless data traffic has drastically increased due to a change in the way today's society creates, shares and consumes information. In 2016, the need to provide wireless connectivity to *anything*, *anywhere*, *anytime* has resulted in more than 8.6 billion mobile devices connected to the Internet, which have generated a total of 11.5 exabytes per month of mobile data traffic [1]. Moreover, estimates forecast that there will be 12.3 billion mobile-connected devices by 2022. This change has been accompanied by an increasing demand for higher speed wireless communication anywhere, anytime. Following this trend, wireless Terabit-per-second (Tbps) links are expected to become a reality within the next five to ten years [2]. In this context, Terahertz (THz)-band (0.1–10 THz) communication is envisioned as a key technology to satisfy the need for such very high data-rates, both in traditional networking paradigms as well as in novel nanoscale communication networks [2]–[4].

For many decades, the lack of compact high-power signal sources and high-sensitivity detectors able to work at room temperature has hampered the use of the THz band for any application beyond sensing. However, many recent advancements with different technologies is finally closing the so-called THz gap. For example, on the one hand, in an *electronic approach*, III-V semiconductor technologies have demonstrated record performance in terms of output power, noise figure, and power-added efficiency at sub-THz frequencies, and are quickly approaching the 1 THz mark [5]–[7]. On the other hand, in an *optics or opto-electronic approach*, Quantum Cascade Lasers are rising as potential candidates for high-power THz-band signal generation [8]–[11]. More recently, the use of nanomaterials such as graphene is enabling the development of novel plasmonic transceivers and antennas, which intrinsically operate in the THz-band [12]–[15].

The THz band provides wireless communication devices with an unprecedentedly large bandwidth, ranging from several tens of GHz up to a few THz [16], [17]. The main phenomenon affecting the propagation of THz-band signals is the absorption by water vapor molecules. For communication distances below one meter, where the number of molecules found along the path is small, the THz band behaves as a single transmission window several THz wide. This very large bandwidth has motivated the use of very short pulse-based broadband modulations [18].

As the transmission distance increases, molecular absorption defines multiple transmission windows, each of them tens or hundreds of GHz wide. More specifically, as the number of absorbing molecules increases, the absorption peaks become both stronger and wider, a phenomenon that is known as the broadening of the absorption lines [16], [19]. As a result, multiple narrower transmission windows are defined and, thus, the transmission of broadband pulses is no longer recommended. Moreover, the bandwidth of each individual transmission window shrinks with the transmission distance, and can easily by reduced by an order of magnitude when the distance is increased from 1 to 10 meters. While multi-carrier communication systems have been envisioned [20], it is already challenging to create a single carrier signal, yet alone defining multiple tones. Moreover, the limitations of digital-to-analog and analog-to-digital converters (with sampling frequencies approaching 100 Giga-Samples-per-second [21]) discourage the digital generation of an (orthogonal) multi-band system.

In a traditional wireless communication system, the modulation scheme would be set according to the Signal-to-Noise

This work was supported in part by the U.S. National Science Foundation (NSF) under Grants No. CNS-1730148 and CNS-1801857.

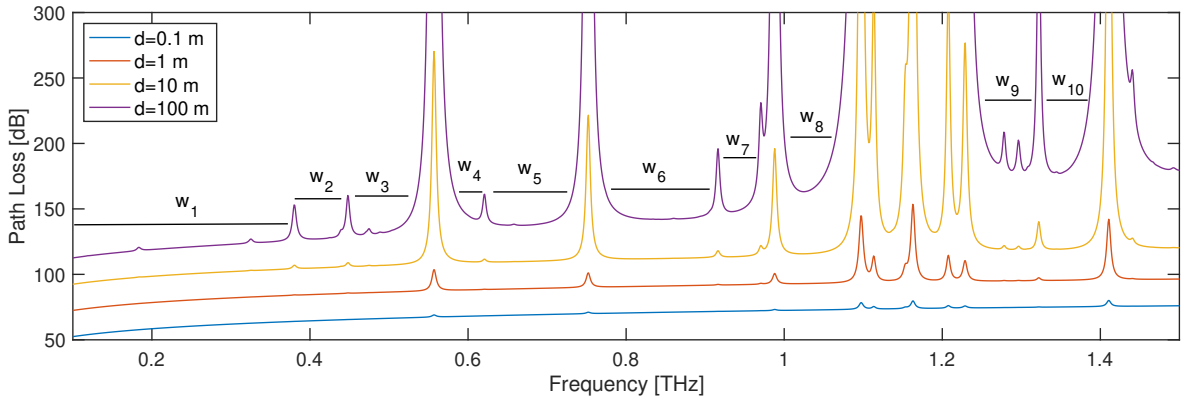


Fig. 1: Path loss in dB at different transmission distances.

Ratio (SNR) of the worst-case (furthest) receiver. Similarly, the bandwidth would be either set by the regulations or, again, by the available bandwidth to the furthest receiver. However, as the bandwidth in the THz band varies with the distance, this modulation scheme will be inefficient in utilizing the high bandwidth available for closer receivers.

To maximize the channel utilization, in this paper we propose hierarchical bandwidth modulations able to cope with the distance-dependent bandwidth of the THz channel. Partially related to the concept of hierarchical or concatenated modulations [22], [23], the fundamental idea in this case is to embed multiple binary information streams on the same carrier signal by manipulating the symbol time. More specifically, for users over short distances, in which the available bandwidth is larger and the path-loss much lower, symbol duration can be made shorter than that for users over longer distances.

After describing possible implementations for the modulator and demodulator, we analytically investigate the performance of the proposed scheme in terms of achievable data rate and compare it to that of traditional hierarchical modulations. In addition, we derive the symbol error rate by starting from the new defined constellations. Finally, we provide extensive numerical results which have been obtained by utilizing an analytical channel model that captures the peculiarities of the THz band. The results show that the proposed modulation scheme can maximize the utilization of the THz band.

The remainder of this paper is organized as follows. In Sec. II, we describe the system model. In Sec. III, we describe the proposed modulation scheme, and we analytically investigate its performance in Sec. IV. We provide numerical results in Sec. V and conclude the paper in Sec. VI.

## II. THz-band Channel Model

The propagation of electromagnetic waves at THz-band frequencies is mainly determined by the spreading loss and the molecular absorption loss. In particular, the path loss for THz-band channel is given by [16] as

$$PL_{LOS}(f,d) = \left(\frac{4\pi f d}{c}\right)^2 e^{k_{abs}(f)d}, \qquad (1)$$

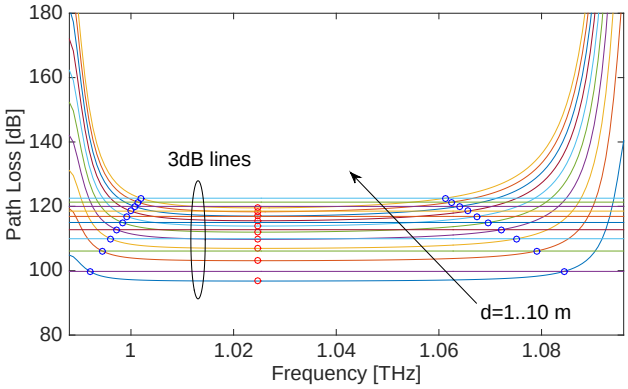


Fig. 2: Available $B_{3dB}$ as function of distance.

where $f$ is the operating frequency, $d$ is the separation between the transmitter and receiver, $c$ is the speed of light in free space and $k_{abs}$ is frequency-dependent absorption coefficient of the medium [16]. In Fig. 1, the path loss in dB according to [16] is shown for different transmission distances, for a standard atmosphere with 40% humidity. This result agrees with the experimental measurements discussed in [24]. There are several observations to be made. First and foremost, molecular absorption plays a key role in defining the available transmission bandwidth. For distances below one meter, the THz band behaves as a single transmission window several THz wide. However, for longer distances, the absorption from water vapor defines multiple transmission windows ($w_1, w_2, w_3$, ... in Fig. 1). The second observation to be made relates to the way in which the absorption loss is captured in analytical models. Traditionally, the absorption loss is given as a constant exponent in dB/km at a given window. However, this masks the fact that the absorption loss also determines the bandwidth, which changes drastically with distance. As the distance increases (i.e., the number of absorbing molecules augments), not only the absorption loss increases, but also the transmission windows shrink. For example, in Fig. 2, we illustrate the normalized path loss for the first transmission window above 1 THz. The plot shows that the available bandwidth can go from 91.55 GHz down to 57.98 GHz when the communication distance increases from 1 m to 10 m.This property motivates

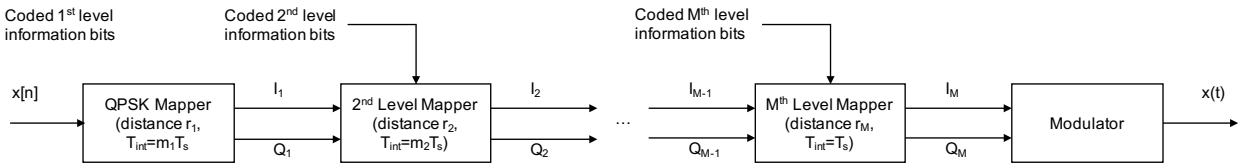


Fig. 3: Block diagram for the hierarchical bandwidth modulator.

the proposed modulation scheme.

## III. Hierarchical Bandwidth Modulation

To maximize the channel utilization, we propose hierarchical bandwidth modulation (HBM) able to cope with the distance-dependent bandwidth at THz-band frequencies. The advantage of our scheme comes from exploiting the molecular absorption for user spatial multiplexing.

### A. Modulator and Demodulator

The conceptual block diagram of the hierarchical bandwidth modulation for THz band communication is shown in Fig. 3. The figure depicts an M-level modulator in which a QPSK modulation is chosen to be the base layer modulation and $r_1 > r_2 > r_3 > ... > r_M$, where $r_i$ is the distance between the transmitter and the $i$th receiver.

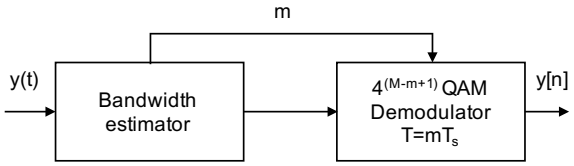


Fig. 4: Block diagram for the HBM demodulator.

The outputs of the first block are the I and Q components of the base modulation, which are held constant for a total symbol time of $m_1 T_s$, where $m_1$ is an integer and $T_s$ is the inverse of the bandwidth available at the closest receiver. The second mapping block further modulates the I and Q components according to the second level of information. In other words, each QPSK symbol is further mapped to a local QPSK modulation. In this case, the information bits are held for a total symbol time of $m_2 T_s$. Note that, $m_1$ must be an integer multiple of $m_2$. This is applied successively until the highest level modulation, $M$, whose symbols are held only for Ts. For a fixed transmission power, the fact that higher level modulations are held for shorter times results into a lower transmission energy per bit $E_b$. However, over the shorter distances at which these symbols are expected to be received, the channel path-loss is lower, which results in still high $E_b/N_0$ values at the receiver. On the receiver side, as shown in Fig. 4, the first step is to estimate the bandwidth $\frac{1}{T_s'}$ of the received signal, which in the simplest case could be done by means of a training pulse sequence. Based on the estimated factor $m = T_s'/T_s$, the received signal is then demodulated as a $4^{(M-m+1)}$QAM at a $\frac{1}{mT_s}$ rate. A traditional M-level hierarchical modulator maps all the layers at the same rate that is suitable for the farthest receiver. In the considered scenario, this rate would be $\frac{1}{MT_s}$, where $\frac{1}{T_s}$ is the rate available for closest receiver. On the receiver side, the demodulator would estimate the bandwidth $\frac{1}{T_s'}$ to get an estimate of the distance ($m = T_s'/T_s$) and in turn to decide on the demodulator ($4^{(M-m+1)}$QAM). However, the symbol duration would still be $MT_s$ for all of the $M$ receivers.

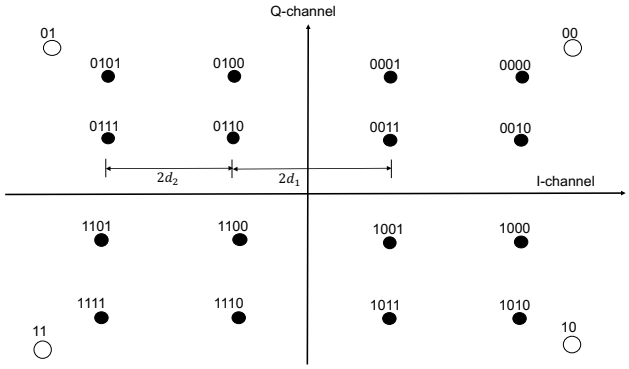


Fig. 5: Constellation diagram for the HBM.

### B. Constellation Diagram

The constellation diagram of our proposed hierarchical modulation looks a bit different from the traditional hierarchical modulation as shown in Fig. 5. As can be seen from the figure, the base layer constellation points are no more inside the clusters. The reason for this is that the symbol duration for enhanced layer information is shorter than that of the base layer. As a result the energy of the base layer symbol is more than the energy of enhanced layer symbols. Nevertheless, the received signal at short distance experiences much less attenuation than the farther receiver which makes it possible for the closer receiver to demodulate at a faster rate.

## IV. Performance Analysis

In this section we first show that the proposed hierarchical bandwidth modulation can achieve higher transmission rates than the traditional hierarchical modulation while using THz band communication. Then we analyze the performance of the proposed modulation in terms of symbol error rate(SER).

### A. Achievable Information Rate

The discrete time Gaussian broadcast channel for two users can be written as follows [25].

$$y_k[m] = h_k[m]x[m] + w_k[m],\ k = 1, 2, \tag{2}$$

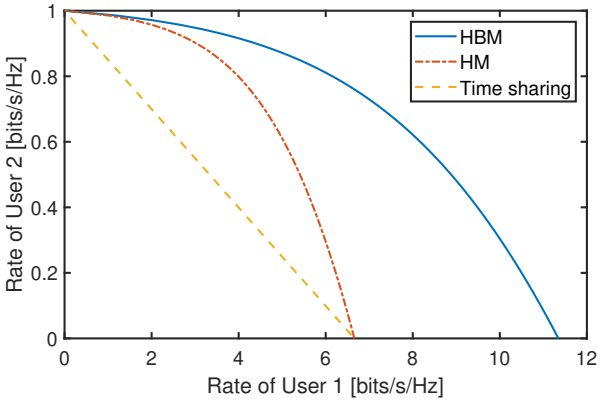


Fig. 6: Achievable rates for traditional HM and HBM.

where $y_k$ is the received signal of user $k$, $h_k$ is the channel between the transmitter and user $k$ and $w_k$ is the noise at receiver $k$. Under the assumption that $|h_1| > |h_2|$ (i.e., user 1 is closer), with each possible power split of $P = P_1 + P_2$, the following rate pair can be achieved [26],

$$\begin{aligned} R_1 &= log\left(1 + \frac{P_1|h_1|^2}{N_o}\right) \\ &+ log\left(1 + \frac{P_2|h_2|^2}{P_1|h_2|^2 + N_o}\right) bits/s/Hz \\ R_2 &= log\left(1 + \frac{P_2|h_2|^2}{P_1|h_2|^2 + N_o}\right) bits/s/Hz \end{aligned} \tag{3}$$

If hierarchical bandwidth modulation is used, the close receiver would have double the bandwidth and the noise. As a result, the achievable rates of the two receivers become

$$\begin{aligned} R_1 &= 2log\left(1 + \frac{P_1|h_1|^2}{2N_o}\right) \\ &+ log\left(1 + \frac{P_2|h_2|^2}{P_1|h_2|^2 + N_o}\right) bits/s/Hz \\ R_2 &= log\left(1 + \frac{P_2|h_2|^2}{P_1|h_2|^2 + N_o}\right) bits/s/Hz \end{aligned} \tag{4}$$

In Fig.6 we show the boundaries of rate regions achievable with bandwidth hierarchical modulation, hierarchical modulation and time sharing schemes for the asymmetric AWGN channel (with $SNR_1 = 20\ dB$ and $SNR_2 = 0\ dB$). As can be seen from the figure, the achievable rate for HBM strictly dominates that of traditional HM.

### *B. Symbol Error Rate*

In this section we investigate the the error performance of the proposed hierarchical bandwidth modulation in AWGN noise for the same two users scenario. In the literature, the SER performance has usually been derived for base information bits and the enhancement layer information bits separately. In this paper, however, we are interested in SER performance at the closer receiver and the farther receiver. For the closer receiver the constellation looks like a regular non-uniform

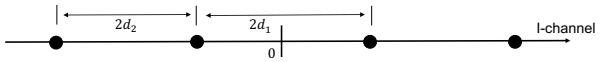


Fig. 7: Constellation diagram for the 4PAM modulation.

16QAM and the resulting SER can be derived considering the 16QAM as the Cartesian product of a one dimensional 4PAM constellation with itself [27]. The corresponding non-uniform 4PAM constellation is shown in Fig. 7. Considering equal probability for each constellation point, The SER can be deduced as follows

$$P_e^{'} = Q\left(\frac{d_2}{\sqrt{\frac{N_0}{2}}}\right) + \frac{1}{2}Q\left(\frac{d_1}{\sqrt{\frac{N_0}{2}}}\right), \tag{5}$$

where $Q(.)$ is the standard Q-function and $P_e^{'}$ is the symbol error rate of the non-uniform 4PAM constellation of Figure 7. The probability of correct detection for the 16QAM is thus

$$P_c = \left(1 - P_e^{'}\right)^2 \tag{6}$$

Hence, the probability of symbol error for 16QAM is

$$\begin{aligned} P_e^{closer} &= 1 - P_c \approx 2P_e^{'} \\ &= 2Q\left(\frac{d_2}{\sqrt{\frac{N_0}{2}}}\right) + Q\left(\frac{d_1}{\sqrt{\frac{N_0}{2}}}\right), \end{aligned} \tag{7}$$

where $P_e^{closer}$ is the symbol error probability for the closer receiver. For the farther receiver, the SER is same as that of the base layer, so we can just use it from the literature [28].

## V. Numerical Results

In this section, we first show the simulation of the proposed HBM and compare it's performance with unicast and classical HM in terms of data rate. The carrier frequency is chosen to be 1.04 THz. Considering that the channel bandwidth is chopped almost to half from 1 m to 30 m distance, we place two receivers at distance 1 m and 30 m. The bandwidth available at the closer and farther receivers is 92 GHz and 45 GHz respectively. We set the transmission power to 10 mW, in light of the existing compact THz sources at room temperature. We consider the transmitter and the receiver to be equipped with directional antennas. We set the appropriate antenna gain to meet the SNR requirement at the furthest receiver. Based on that gain, the resulting SNR on the closest node is determined (see Fig. 10). The modulated signal is passed through the THz channel module, which implements the frequency-dependent model described in Sec. II. The detailed list of parameters used to conduct the simulation are presented in Table I.

In Fig. 8, we illustrate the time and frequency domain representation of the transmitted signal, the received signal at 1 m and the received signal at 30 m, respectively. From this figure, it is clear that not only the received signal power is much lower, but its bandwidth has been drastically reduced. This is due to the high frequency components being chopped by the molecular absorption of THz channel. This phenomenon

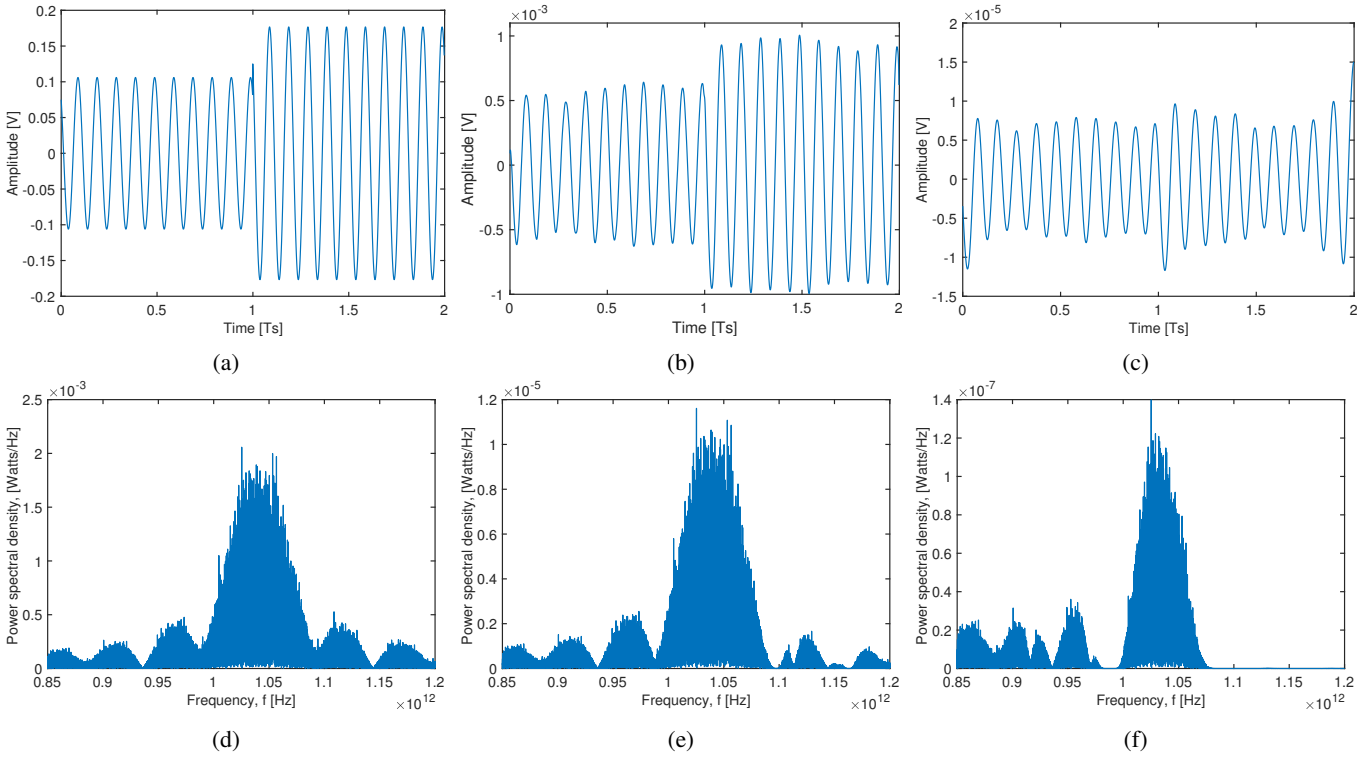


Fig. 8: Time and frequency domain plot of the transmitted signal, received signal at 1 m and received signal at 30 m.

TABLE I: Simulation parameters

| Parameters | Values |
|---|---|
| Carrier frequency | 1.04 THz |
| Frequency window | $w_6$ |
| M | 2 |
| Transmission power | 10 dBm |
| Humidity | 40% |
| Temperature | 293 Kelvin |
| Pressure | 1 atm |
| Antenna gain | 24 dB |

is clearer from the frequency domain plot of the signals in fig. 8d, 8e, and 8f. As a result, the user at 30 m distance can not receive the enhancement layer information, rather bound to demodulate the base layer information at rate $\frac{1}{2T_s}$. The error performance for the closer receiver in additive white Gaussian noise (AWGN) is shown in Fig. 9. This simulation was performed for $\lambda = \frac{d_2}{d_1} = 0.4$. As can be seen from the figure, our analytical result closely follow the simulation results. The slight difference at the low SNR value happens due to the elimination of higher order terms in the derivation of the analytical result. In addition, very high SNR value is required to obtain a useful performance. This is usually the case in the literature for hierarchical modulation. The reason for this is that the constellation points gets much closer than that of the regular 16QAM and increases the chance of a symbol being erroneous. However, as shown in Fig. 10 , the received SNR for the closer receiver is very high for even a small SNR for the farther receiver. This means while channel is good enough for the farther receiver, the closer receiver experiences very reliable

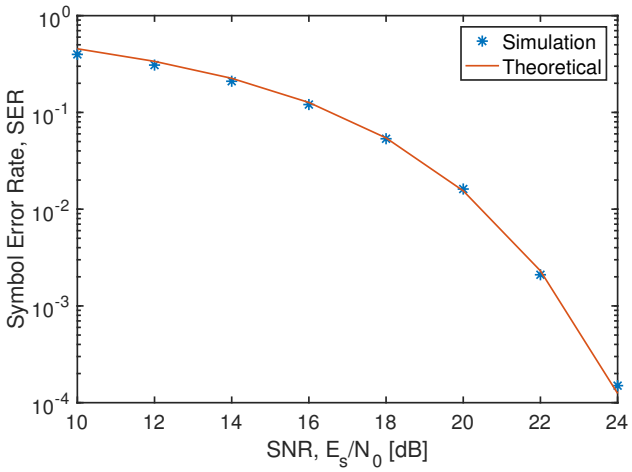


Fig. 9: SER as a function of SNR for closer receiver.

channel conditions. To show this more clearly, the SER for both closer and farther receiver has been depicted in Fig. 11 as function of the SNR for farther receiver. As can be seen from this figure, the closer receiver has no error until the SNR for farther receiver goes as bad as -6 dB which would never be the target. To see this better, the received constellation diagrams at the closer and farther receiver is shown in Fig. 12 and Fig. 13 respectively for an SNR of 18 dB at the farther node.

To compare the data rate, the bit error rates of hierarchical bandwidth modulation and other alternatives have been depicted in Table II for the same transmit power and antenna gain

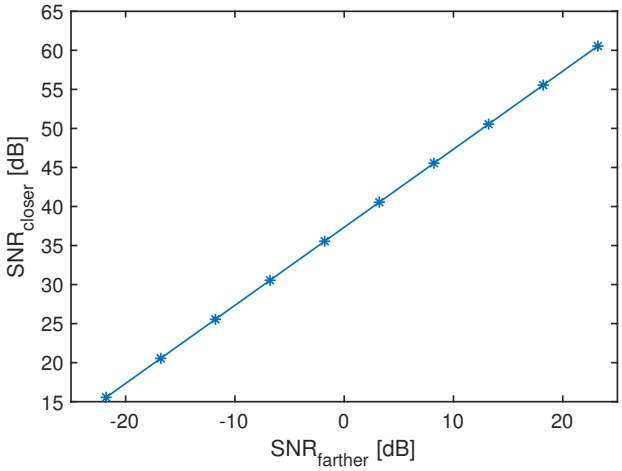


Fig. 10: SNR of closer receiver as a function of SNR of farther receiver.

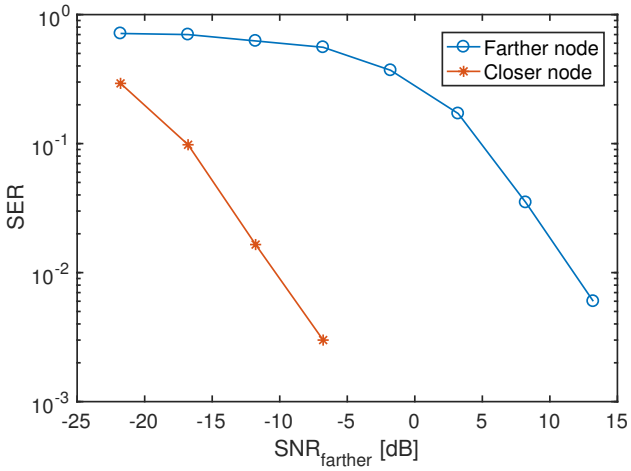


Fig. 11: SER of both closer and farther receiver as a function of SNR of farther receiver.

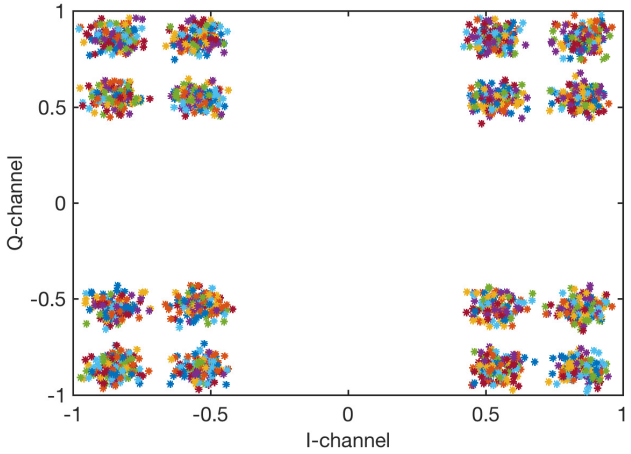


Fig. 12: Received constellation at closer receiver.

mentioned above. The noise power was calculated according to the bandwidth used by the modulation schemes and the

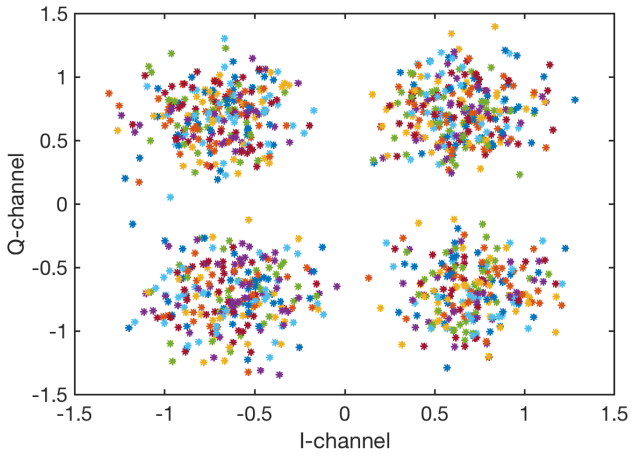


Fig. 13: Received constellation at farther receiver.

noise model in [18]. As can be seen from the table, if unicast modulation is used, QPSK is the only one that can achieve the required BER of $10^{-3}$ for the farther receiver. For the closer receiver, upto 256QAM can be used and 1024QAM introduces high error rate. To maximize the throughput and meet the BER requirement at the same time, 256QAM is used for closer receiver with symbol rate $\frac{1}{T_s}$ and QPSK is used for farther receiver with symbol rate $\frac{1}{2T_s}$. Hence, considering that one user is served at a time in unicast scheme, the data rate for closer receiver and farther receiver are $\frac{8bits}{T_s}$(256QAM) and $\frac{2bits}{2T_s}$(4QAM) respectively. Hence, the average data rate is

$$\frac{10bits}{3T_s} = \frac{3.33bits}{T_s} = .307\text{Tbps} \tag{8}$$

Traditional hierarchical modulation uses the bandwidth available to the farther receiver and serves the users at the same time. As can be seen from the table, a 4/64QAM scheme can meet the BER requirement. Hence the throughput in this case can be calculated as

$$\frac{6bits}{2T_s} + \frac{2bits}{2T_s} = \frac{8bits}{2T_s} = \frac{4bits}{T_s} = .370\text{Tbps} \tag{9}$$

Hierarchical bandwidth modulation adjusts the symbol duration according to the available bandwidth. A 4/16QAM scheme meets the BER requirement for hierarchical bandwidth modulation. Accordingly, the throughput can be calculated as

$$\frac{8bits}{2T_s} + \frac{2bits}{2T_s} = \frac{10bits}{2T_s} = \frac{5bits}{T_s} = .462\text{Tbps} \tag{10}$$

As can be deduced from the above numerical analysis, hierarchical bandwidth modulation outperforms the existing modulation schemes by approximately 25% in THz channel.

## VI. Conclusion

In this paper, we have presented a modulation scheme for THz band communication that takes advantage of the distance dependent bandwidth of THz channel. The proposed scheme is partially related to the hierarchical modulation, but the symbol

TABLE II: BER comparison of different modulation schemes in THz band channel

| Modulation scheme | SER [distance=1m] | SER [distance=30m] | BER [distance=1m] | BER [distance=30m] |
|---|---|---|---|---|
| QPSK | <1e-4 | <1e-4 | <1e-4 | <1e-4 |
| 16QAM | <1e-4 | 0.01 | <1e-4 | 2.5e-3 |
| 64QAM | <1e-4 | 0.30 | <1e-4 | 0.05 |
| 256QAM | <1e-4 | 0.73 | <1e-4 | 0.09 |
| 1025QAM | 0.14 | 0.93 | 0.014 | 0.09 |
| 4/16HM, $\lambda = 0.25$ | <1e-4 | 5.5e-4 | <1e-4 | 2.75e-4 |
| 4/16HM, $\lambda = 0.2$ | <1e-4 | 3e-4 | <1e-4 | 1.5e-4 |
| 4/64HM, $\lambda = 0.125$ | <1e-4 | 0.003 | <1e-4 | 1.5e-3 |
| 4/64HM, $\lambda = 0.0625$ | 0.02 | 1e-3 | 3.3e-3 | 5e-4 |
| 4/64HM, $\lambda = 0.0825$ | 3e-4 | 0.0016 | 5e-5 | 8e-4 |
| 4/16HBM, $\lambda = 0.25$ | <1e-4 | 1e-3 | <1e-4 | 5e-4 |
| 4/16HBM, $\lambda = 0.2$ | 4e-4 | 6e-4 | 1e-4 | 3e-4 |

time is adjusted according to the available bandwidth at distance. We have shown that the proposed solution outperforms the classical hierarchical modulation in terms of achievable rates. In addition we have derived the symbol error probability for the closer receiver in AWGN channel and compared with the simulation results to show the validity of the analytical result. Finally, the bandwidth hierarchical modulated signal was simulated and passed through THz channel to show how the proposed solution is able to take advantage of the distance dependent bandwidth. As part of our future work, we will extend this work for more than two receivers and optimize the performance of the proposed modulation scheme.

## REFERENCES


[1] Cisco, "Cisco visual networking index: Global mobile data traffic forecast update, 2017–2022," *White Paper*, Feb. 2019.

[2] I. F. Akyildiz, J. M. Jornet, and C. Han, "Terahertz band: Next frontier for wireless communications," *Physical Communication (Elsevier) Journal*, vol. 12, pp. 16–32, Sep. 2014.

[3] H.-J. Song and T. Nagatsuma, "Present and future of terahertz communications," *IEEE Transactions on Terahertz Science and Technology*, vol. 1, no. 1, pp. 256–263, 2011.

[4] T. Kurner and S. Priebe, "Towards THz Communications-Status in Research, Standardization and Regulation," *Journal of Infrared, Millimeter, and Terahertz Waves*, vol. 35, no. 1, pp. 53–62, 2014.

[5] S. Koenig, D. Lopez-Diaz, J. Antes, F. Boes, R. Henneberger, A. Leuther, A. Tessmann, R. Schmogrow, D. Hillerkuss, R. Palmer *et al.*, "Wireless sub-THz communication system with high data rate," *Nature Photonics*, vol. 7, no. 12, pp. 977–981, 2013.

[6] Y. Kurita, G. Ducournau, D. Coquillat, A. Satou, K. Kobayashi, S. B. Tombet, Y. Meziani, V. Popov, W. Knap, T. Suemitsu *et al.*, "Ultrahigh sensitive sub-terahertz detection by InP-based asymmetric dual-grating-gate high-electron-mobility transistors and their broadband characteristics," *Applied Physics Letters*, vol. 104, no. 25, p. 251114, 2014.

[7] V. Radisic, K. Leong, D. Scott, C. Monier, X. Mei, W. Deal, and A. Gutierrez-Aitken, "Sub-millimeter wave InP technologies and integration techniques," in *IEEE MTT-S International Microwave Symposium (IMS)*, May 2015, pp. 1–4.

[8] B. S. Williams, "Terahertz quantum-cascade lasers," *Nature photonics*, vol. 1, no. 9, pp. 517–525, 2007.

[9] Q. Lu, S. Slivken, N. Bandyopadhyay, Y. Bai, and M. Razeghi, "Widely tunable room temperature semiconductor terahertz source," *Applied Physics Letters*, vol. 105, no. 20, p. 201102, 2014.

[10] Q. Lu, D. Wu, S. Sengupta, S. Slivken, and M. Razeghi, "Room temperature continuous wave, monolithic tunable THz sources based on highly efficient mid-infrared quantum cascade lasers," *Scientific reports*, vol. 6, 2016.

[11] S. Slivken and M. Razeghi, "High power, electrically tunable quantum cascade lasers," in *SPIE OPTO*. International Society for Optics and Photonics, 2016, pp. 97 550C–97 550C.

[12] K. S. Novoselov, V. Fal, L. Colombo, P. Gellert, M. Schwab, K. Kim *et al.*, "A roadmap for graphene," *Nature*, vol. 490, no. 7419, pp. 192–200, 2012.

[13] A. C. Ferrari, F. Bonaccorso, V. Fal'Ko, K. S. Novoselov, S. Roche, P. Bøggild, S. Borini, F. H. Koppens, V. Palermo, N. Pugno *et al.*, "Science and technology roadmap for graphene, related two-dimensional crystals, and hybrid systems," *Nanoscale*, vol. 7, no. 11, pp. 4598–4810, 2015.

[14] J. M. Jornet and I. F. Akyildiz, "Graphene-based plasmonic nano-antenna for terahertz band communication in nanonetworks," *IEEE JSAC, Special Issue on Emerging Technologies for Communications*, vol. 12, no. 12, pp. 685–694, Dec. 2013.

[15] ——, "Graphene-based plasmonic nano-transceiver for terahertz band communication," in *Proc. of European Conference on Antennas and Propagation (EuCAP)*, 2014.

[16] ——, "Channel modeling and capacity analysis of electromagnetic wireless nanonetworks in the terahertz band," *IEEE Transactions on Wireless Communications*, vol. 10, no. 10, pp. 3211–3221, Oct. 2011.

[17] S. Priebe and T. Kurner, "Stochastic modeling of THz indoor radio channels," *IEEE Transactions on Wireless Communications*, vol. 12, no. 9, pp. 4445–4455, 2013.

[18] J. M. Jornet and I. F. Akyildiz, "Femtosecond-long pulse-based modulation for terahertz band communication in nanonetworks," *IEEE Transactions on Communications*, vol. 62, no. 5, pp. 1742–1754, May 2014.

[19] R. M. Goody and Y. L. Yung, *Atmospheric Radiation: Theoretical basis*, 2nd ed. Oxford University Press, 1989.

[20] C. Han, A. O. Bicen, and I. F. Akyildiz, "Multi-wideband waveform design for distance-adaptive wireless communications in the terahertz band," *IEEE Transactions on Signal Processing*, vol. 64, no. 4, pp. 910–922, Feb. 2016.

[21] Fujitsu. 56GSa/s 8-bit Analog-to-Digital Converter. [Online]. Available: http://www.fujitsu.com/downloads/MICRO/fma/pdf/56G_ADC_Fact-Sheet.pdf

[22] H. Jiang, P. Wilford *et al.*, "A hierarchical modulation for upgrading digital broadcast systems," *IEEE Transactions on Broadcasting*, vol. 51, no. 2, pp. 223–229, 2005.

[23] K. Ramchandran, A. Ortega, K. M. Uz, and M. Vetterli, "Multiresolution broadcast for digital hdtv using joint source/channel coding," *IEEE journal on Selected Areas in Communications*, vol. 11, no. 1, pp. 6–23, 1993.

[24] Y. Yang, A. Shutler, and D. Grischkowsky, "Measurement of the transmission of the atmosphere from 0.2 to 2 thz," *Optics express*, vol. 19, no. 9, pp. 8830–8838, 2011.

[25] D. Tse and P. Viswanath, *Fundamentals of wireless communication*. Cambridge university press, 2005.

[26] T. Cover, "Broadcast channels," *IEEE Transactions on Information Theory*, vol. 18, no. 1, pp. 2–14, 1972.

[27] S. S. Haykin, *Digital Communication Systems*. Wiley New York, 2014, vol. 1.

[28] K. Fazel and M. Ruf, "Combined multilevel coding and multiresolution modulation," in *Communications, 1993. ICC'93 Geneva. Technical Program, Conference Record, IEEE International Conference on*, vol. 2. IEEE, 1993, pp. 1081–1085.